Hindawi
Shock and Vibration
Volume 2021, Article ID 9538647, 11 pages
https://doi.org/10.1155/2021/9538647

Research Article

Aerodynamic Performance of Propellers for Multirotor Unmanned Aerial Vehicles: Measurement, Analysis, and Experiment

Hang Zhu[1] **Zihao Jiang**[1] **Hang Zhao**[1] **Siyu Pei**[1] **Hongze Li**[1] **and Yubin Lan**[2,3]

[1]*Key Laboratory of CNC Equipment Reliability, Ministry of Education, School of Mechanical and Aerospace Engineering, Jilin University, Changchun 130025, China*
[2]*College of Electronic Engineering, South China Agricultural University, Guangzhou 510642, China*
[3]*National Center for International Collaboration Research on Precision Agricultural Aviation Pesticides Spraying Technology, Guangzhou 510642, China*

Correspondence should be addressed to Hang Zhu; hangzhu@jlu.edu.cn and Yubin Lan; ylan@scau.edu.cn

Received 2 July 2021; Accepted 23 August 2021; Published 22 September 2021

Academic Editor: Lei Hou

Analyzing the propeller aerodynamic performance is of vital importance for research and improvement of unmanned aerial vehicles. This paper presents the design requirements for a propeller for rotorcraft unmanned aerial vehicles and an analysis of a model for calculating propeller aerodynamic performance. Based on blade element momentum theory, the aerodynamic force of a blade element is analyzed and used. The symmetric airfoil NACA 0012 is used as an example to verify the validity of the model. An experimental system for propeller aerodynamic performance is designed and built to test the aerodynamic performance of six types of the propeller from a single manufacturer (APC). Data-processing software is also developed to draw curves and perform single-step calculations of three propellers' parameters: airfoil resistance power, induced velocity, and efficiency. The results of the experiment indicate that both the thrust and torque of the propeller increase with rotational speed, propeller diameter, and propeller pitch. The research is of great significance to select more suitable propellers for unmanned aerial vehicles and the further improvement of the performance of unmanned aerial vehicles' dynamical system.

1. Introduction

UAVs (unmanned aerial vehicles) have the characteristics of being aircraft with simple operation, high reliability, good maintainability, high flexibility, and high-performance feedback controllers [1]. UAVs have been widely used in recent years in plant protection operations [2], remote sensing [3–5], medical and health care sectors, military reconnaissance, express logistics, emergency rescue, environmental management, mining operations [6], infrastructure development, and other fields [7]. The complex and varied work requires higher performance of UAVs, which makes it essential to analyze the aerodynamic performance of UAVs.

The power of multirotor UAVs is derived from the lift generated by the rotation of its propellers. To change the attitude and working state of UAVs, its electronic drivers are used to control the speed and, therefore, the thrust generated in each propeller. Analyze and quantify the controllability about hovering through principle model discussions [8]. Fault diagnosis is performed by applying multilayer adaptation convolutional neural network, and hierarchical representations are learnt from the collected signals [9]. The power of gasoline-powered UAVs is derived from their engines, the output speed of which is essentially constant [10]. The flight attitude of such UAVs is modified by adjusting rotor pitch, thus changing the lift of each rotor [11]. Therefore, the propeller is the most important component to determine the performance of the UAVs and the efficiency of its propulsion system [12–14]. Monospinner is an aircraft with only one propeller as the moving part. After eliminating the yaw state, its linearization system can be controlled horizontally and vertically in position [15]. In addition to blade radius, the propeller speed and pitch also have a significant impact on the performance of UAVs. For analysis of propeller performance, the classical theory of blade element momentum theory [16, 17] has been widely used to evaluate the aerodynamic characteristics of propellers. To guarantee that the theoretical calculations agree closely with the real values, various modified blade element momentum theories have been developed. These modifications include abandoning the small inflow angle assumption [18, 19] and considering the tip vortex [20–22]. In addition to computational fluid dynamics (CFD) simulations [23, 24], experimental platforms are also selected to determine the aerodynamic performance of propellers. A position estimation method using sensor fusion in a structured environment is developed to obtain the localization states of the UAVs [25]. A simple experimental platform was used to test small two- or three-blade propellers with fixed pitch [26]; a variable-pitch propeller experimental platform has also been used [27]. Furthermore, some researchers have conducted wind tunnel tests [28–31]. There has been some analysis of the aerodynamic performance of UAVs, but relatively little analysis related to the influence of propeller parameters on its aerodynamic performance parameters.

The rest of the paper is organized as follows. In Section 2, we analyze the aerodynamic performance of propellers based on blade element momentum theory, establish a calculation model for the selection of blade parameters for multirotor UAVs, and then choose symmetric airfoil NACA 0012 as an example to verify the feasibility and rationality of the model. In Section 3, we describe an experimental platform designed to test the aerodynamic performance of small propellers, which is used to explore the variation of thrust, torque, and static thrust coefficient C_{T0} with diameter, pitch, and speed, and the relationship among these variables. In Section 4, we provide the conclusions along with the significance of this work and future research.

2. Calculation of Propeller Aerodynamic Performance

2.1. Blade Element Momentum Theory. We use blade element momentum theory as the theoretical basis for studying the aerodynamic performance of UAV propellers. The blade of a propeller can be divided into infinite number of continuous elements along its chord length, and the aerodynamic forces on a blade can be analyzed by analyzing the differential forces of the elements [32, 33]. Summing the aerodynamic forces of each blade element gives the aerodynamic force of the whole blade.

The parameters, velocities, and forces of a blade element are shown in Figure 1, where V_{up} is the speed at which the drone takes off vertically, V_i is the induced velocity, $\Omega \cdot r$ is the linear velocity of the blade element at the position where the radius is r, at the axis of the propeller, $r = 0$, the linear velocity is 0, and the tip of the propeller is $r = R$, the linear velocity is $\Omega \cdot R$, where Ω is the rotor angular velocity and R is the propeller radius, W is the relative air velocity, α is the angle of attack, φ is the pitch angle, and ε is the inflow angle.

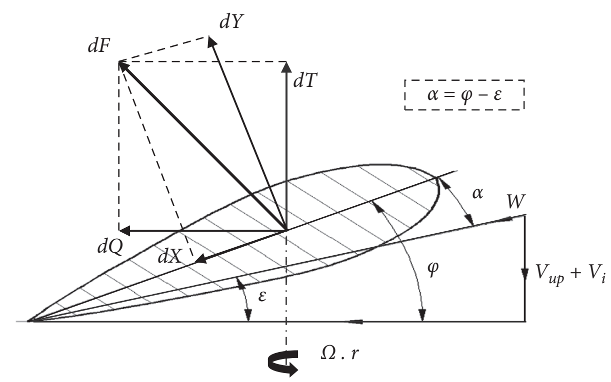

Figure 1: Parameters, velocities, and forces of a blade element.

As shown in Figure 1, W can be calculated according to the following equation:

$$W = \left(V_{\text{up}} + V_i\right) + \Omega R. \tag{1}$$

Aerodynamic performance mainly refers to the lift, resistance, and power generated by the blade during the working process. The lift, C_l, and drag coefficients, C_d, are needed to calculate the lift and drag generated by blades according to blade element momentum theory. They are defined as

$$C_l = \frac{Y}{1/2\rho W^2 S}, \tag{2}$$

$$C_d = \frac{X}{1/2\rho W^2 S}, \tag{3}$$

where ρ is the air density, S is the effective area of the blade element, Y is the airfoil lift, and X is the airfoil drag.

S can be calculated according to

$$S = b \cdot \Delta r, \tag{4}$$

where b is the length of the chord and Δr is the length of the blade element.

The characteristic curves for lift and resistance can be created once the airfoil has been determined. C_l and C_d are determined for the lift and resistance curves, respectively, according to α and the Reynolds number Re

$$\text{Re} = \frac{\rho v_f l}{\mu}, \tag{5}$$

where v_f is the freestream velocity, μ is the kinetic viscosity, and l is the characteristic dimension, which is usually defined as either local chord length or chord length at 75% of radius. Therefore, the differential lift of the element, dY, and drag of the element, dX, can be calculated according to equations (2) and (3), as

$$\begin{aligned} \mathrm{d}Y &= \left(C_l \frac{1}{2}\rho W^2 b\right)\mathrm{d}r, \\ \mathrm{d}X &= \left(C_d \frac{1}{2}\rho W^2 b\right)\mathrm{d}r. \end{aligned} \tag{6}$$

Furthermore, the net force on the blade element along the rotation axis, dT, the net force on the blade element along the vertical rotation axis, dQ, and the lift force, T, and drag force, Q, generated by a single blade can be calculated as

$$\begin{aligned} dT &= \cos(\varepsilon)dY - \sin(\varepsilon)dX, \\ dQ &= \sin(\varepsilon)dY - \cos(\varepsilon)dX, \\ T &= \int_{R_0}^{R} dT, \\ Q &= \int_{R_0}^{R} dQ. \end{aligned} \quad (7)$$

For calculating the propeller power, the required power, P_R, includes the induced rotation resistance power, P_i, the airfoil resistance power, P_0, the waste resistance power, P_p, and the amount of power UAVs uses to overcome gravity during vertical takeoff, P_m:

$$P_i = T \cdot V_i, \quad (8)$$

$$P_0 = nQL\Omega, \quad (9)$$

$$\begin{aligned} P_p &= Q_{air} V_{forward}, \\ P_m &= mgV_{up}, \end{aligned} \quad (10)$$

where n is the number of blades per rotor, L is the distance between the point of action of the rotation resistance and the propeller shaft, Q_{air} is the freestream resistance, $V_{forward}$ (as distinct from v_f) is the cruising speed of the rotary-wing UAVs, and m is the mass of the maximum takeoff weight of the UAVs.

Combined with the above theory, we establish a calculation model for the selection of blade parameters for multirotor UAVs by comparing the maximum thrust and the takeoff weight of the UAVs, and write a calculation program in the C language. The model of propeller aerodynamic performance can determine feasible ranges for R and b on the basis of the airfoil and m. The calculation flowchart of the model is shown in Figure 2.

In Figure 2, M is the Mach number and V_i can be calculated, based on slipstream theory, as

$$V_i = \sqrt{\frac{T_{single}}{2\rho\pi\left(R^2 - R_0^2\right) \times a}}, \quad (11)$$

where R_0 is the distance between the propeller shaft and the propeller root and a (as distinct from α) is a correction coefficient to compensate for the loss of thrust due to the presence of a narrow ring at the tip of the paddle.

2.2. Example Calculation. In this paper, NACA 0012 symmetrical airfoil [34] is analyzed to determine whether the preset values of R and b are feasible according to our model. The required airfoil parameters can be found on the NACA website. The lift characteristic curve of the airfoil under different Reynolds numbers is shown in Figure 3.

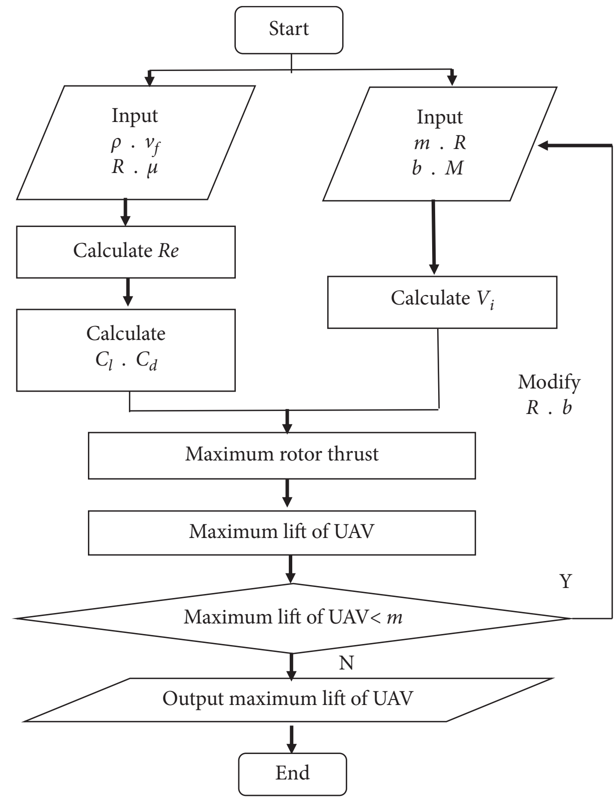

Figure 2: Calculation flowchart of the model.

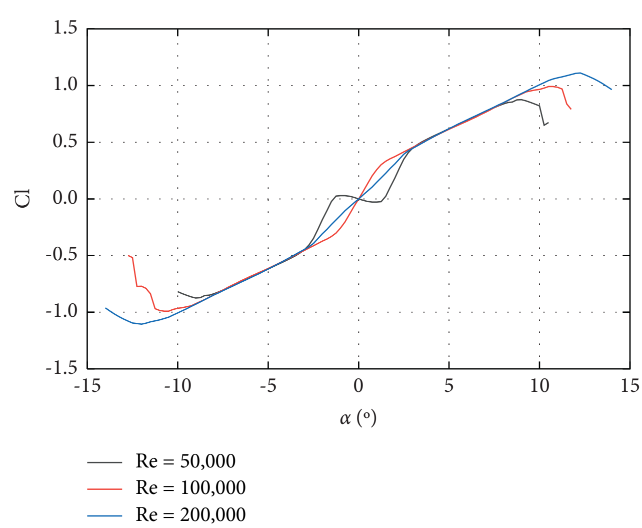

Figure 3: Lift characteristic curve of NACA 0012 airfoil. C_l: lift coefficient; α: angle of attack; Re: Reynolds number.

The atmospheric composition is preset, where $\rho = 1.225\ \text{kg/m}^3$, $v_f = 2\ \text{m/s}$, and $\mu = 1.8247 \times 10^{-5}\ \text{Pa·s}$. Re is calculated based on equation (5):

$$\text{Re} = \frac{\rho v l}{\mu} = \frac{1.225 \times 2 \times (0.4 \times 2)}{1.8247 \times 10^{-5}} = 107414.9175. \quad (12)$$

Refer to Figure 3 and consider the curve for Re = 100,000. When $\alpha = 5°$, we have $C_l = 0.6141$, $C_d = 0.01674$, and the maximum lift-drag ratio, $C_l/C_d = 36.68$. When $\alpha = 10.75°$, we have the maximum values of $C_l = 0.9917$ and $C_d = 0.05469$.

Setting $m = 50$ kg, we get the best lift-drag characteristics at $\alpha = 5°$. When $\alpha = 5°$, by setting $R = 0.4$ m, $b = 0.04$ m, $M = 0.513979$, and $a = 0.99$, we can calculate the thrust generated by a single rotor, $T_{single,}$ in the vertical takeoff state as

$$T_{single} = \frac{mg}{4} = \frac{50 \times 9.8}{4}\,\text{N} = 1.225\,\text{N}. \tag{13}$$

V_i in this state can be calculated as

$$\begin{aligned} V_i &= \sqrt{\frac{T_{single}}{2\rho\pi\left(R^2 - R_0^2\right) \times 0.99}} \\ &= \sqrt{\frac{122.5}{2 \times 1.225 \times \pi \times \left(0.4^2 - 0.052^2\right) \times 0.99}} \\ &= 10.11\,\text{m/s}, \end{aligned} \tag{14}$$

and T_{single} as

$$\begin{aligned} T_{single} = 2 \times \int_{R_0}^{R} &\left(\frac{1}{2} \times C_l \times \rho \times W^2 \times b \times \cos(\varepsilon) - \frac{1}{2} \times C_d \right. \\ &\left. \times \rho \times W^2 \times b \times \sin(\varepsilon)\right) \mathrm{d}r, \end{aligned} \tag{15}$$

so that the lift of the whole UAV, T_{tol}, is calculated as

$$T_{tol} = 4 \times T_{single}. \tag{16}$$

The calculation results are shown in Table 1. T_{tol} in Table 1 is the lift for the whole UAV.

The calculation results show that the selected blade parameters ensure that $T_{tol} \approx mg$ in the hover state and $T_{tol} > mg$ during vertical takeoff, whether $\alpha = 5°$ or $10.75°$. Therefore, the preset values of R and b are feasible.

3. Propeller Aerodynamic Performance Test

3.1. Experimental System Design. The experimental system for propeller aerodynamic performance that we designed and reported in this paper can collect data on propeller speed, T_{single}, and propeller torque. It requires manual operation via a remote control to vary the rotation speed of the blade and consists of two parts: the experimental platform and the measurement and control system. Figure 4 shows the overall design of the system.

A photograph of the experimental system is shown in Figure 5. The experimental platform built on an aluminum alloy frame is used for installing the propeller under test, comprising a brushless motor, force sensor, infrared speed sensor, and other equipment. The propellers on the multirotor are vertically arranged. The propeller in the experimental system is designed to be placed horizontally to eliminate the ground effect.

Table 1: Calculation results.

Flight status	α (°)	T_{single} (N)	T_{tol} (N)
Hover	5	122.5001	490.0006
	10.75	197.3495	789.3980
Vertical takeoff ($V_{up} = 2$ m/s)	5	122.6716	490.6865
	10.75	197.5310	790.1240

We have used two sensors, S-type force sensor and photoelectric speed sensor, and the parameters are shown in Table 2.

As shown in Figure 6, the force measurement sensors are divided into two groups: torque sensors, placed vertically, and thrust sensors, placed horizontally.

As shown in Figure 7, the torque is measured indirectly by sensors arranged symmetrically on the left and right sides. During the experiment, the torque generated by the propeller is transferred to the sensors through the roof plate so that the sensors on each side are subject to the same tension and pressure. The distance between the force sensors on the left and right sides is the length of the moment arm. The product of the measured torsional force and the length of the moment arm (45 mm) is equal to the torque produced by the propeller.

As shown in Figure 8, to measure thrust, the thrust generated by the propeller is transferred to the moving plate through the roof plate. After the moving plate is stressed, it moves backwards along the guide rail and transfers the thrust to the S-type thrust sensor arranged horizontally towards the rear of the experimental platform.

An infrared speed sensor measures the motor speed. In addition, the experimental platform includes a DC stabilized voltage power supply for the brushless motor.

The measurement and control system is used to measure the speed of the brushless motor and the thrust according to the force sensor. The measurement and control system communicates with the computer through a serial port using a data acquisition card. The data on propeller speed, T_{single}, and propeller torque are collected and saved by a LabVIEW program as an Excel file.

To further analyze the data obtained from the aerodynamic performance experiment, data processing software is designed, based on Visual Basic.NET, to provide rapid analysis. The software has two functions:

(i) Reading the propeller speed, thrust, and torque data collected by the data acquisition card and generating the thrust speed and torque speed graphs for the propeller to show the trends, while the speed is varied

(ii) Calculating propeller power, efficiency, and V_i, based on user input of the thrust, torque, and speed

The user interface of the data processing software is shown in Figure 9.

L is difficult to calculate, so P_0 was not calculated using equation (9). The input torque, T_0, and speed, n_0, can be used to calculate P_0 as follows:

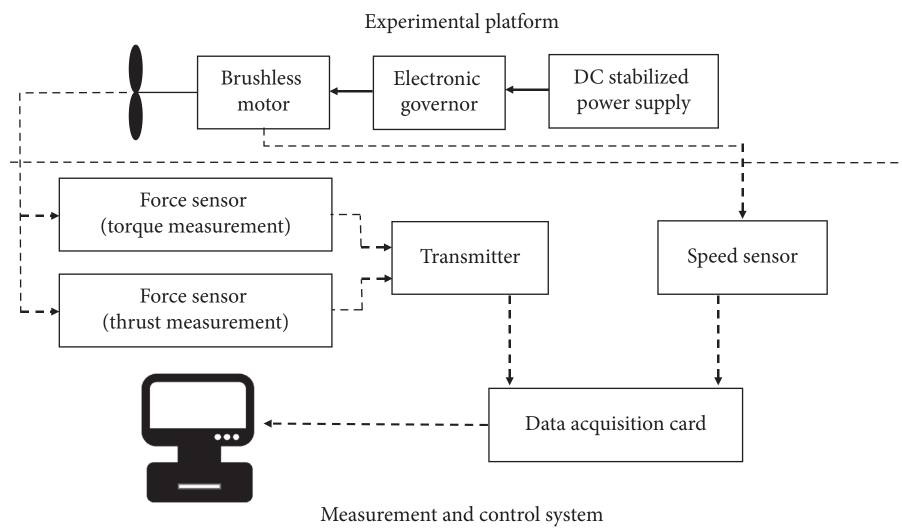

Figure 4: Overall design of the experimental system.

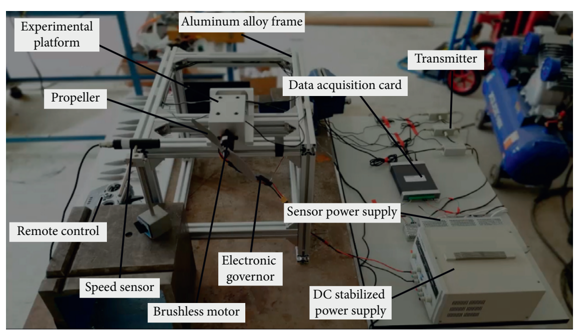

Figure 5: Photograph of the experimental system.

Table 2: Sensor parameters.

Sensor type	S-type force sensor	Photoelectric speed sensor
Range	0~8 kg	—
Working voltage	DC 10~15 V	DC 10~30 V
Operating temperature	−20°C~+80°C	−10°C~+55°C
Output voltage signal	−10~+10 V The positive voltage value represents the pressure of the sensor, and the negative voltage value represents the tension of the sensor	High level 5 V ± 0.5 V Low level < ±0.5 V
Insulation resistance	≥5000 MΩ	≥50 MΩ

$$P_0 = \frac{T_0 \times n_0 \times 1000}{9550}. \quad (17)$$

V_i can be calculated by equation (11), and P_i can be calculated by equation (8).

The efficiency of the propeller, η, can be calculated as

$$\eta = \frac{P_i}{P_i + P_0}. \quad (18)$$

3.2. Analysis of Experimental Results. The purpose of this experiment is to explore how propeller thrust and torque vary with rotational speed. The following six types of propellers, manufactured by APC [35], with different diameters and pitch, are selected for aerodynamic performance testing: APC 8045, APC 9045, APC 9060, APC 9075, APC 1145, and APC 1245. APC is an American company known for producing high-quality propellers. Taking APC 9045 as an example, the first two digits (90) represent that the diameter

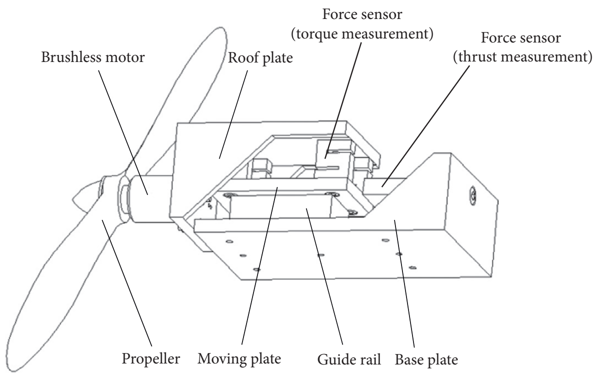

Figure 6: Structure of the experimental platform.

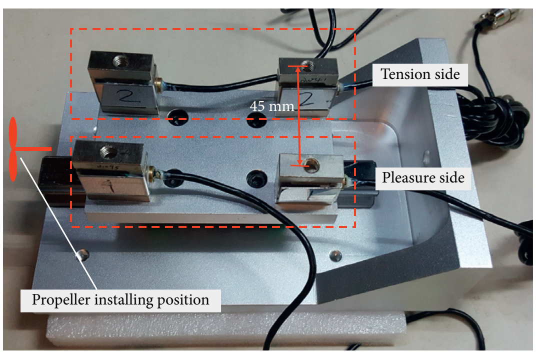

Figure 7: The sensor arrangement to measure the torque.

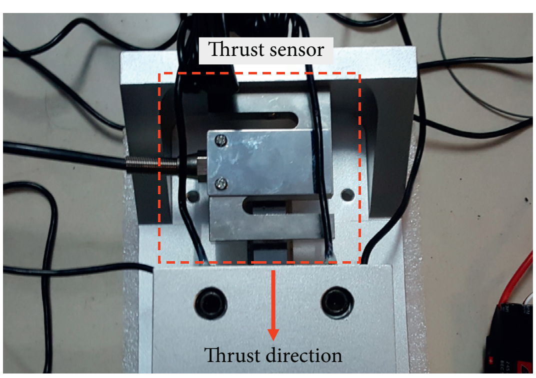

Figure 8: The sensor arrangement to measure the thrust.

is 9.0 inches (228.6 mm), and the last two digits (45) represent that the pitch is 4.5 inches (114.3 mm). All of the propellers belong to the MR series made from carbon fiber.

In this paper, experiments are repeated five times for each propeller to confirm good repeatability. The results of the five repetitions for APC 1145 are shown in Figure 10. The results of the repeated experiments are almost identical, indicating that the experimental platform has good repeatability.

One of the five experimental results is selected for analysis, and the analysis results are as follows.

3.2.1. Effects of Propeller Speed, Diameter, and Pitch on Thrust. Among the propellers tested, those with a pitch of 4.5 inch (114.3 mm), i.e., APC 8045, APC 9045, APC 1145, and APC 1245, were chosen to deduce the effect of diameter on thrust; their parameters are shown in Table 3.

Figure 11 shows the effect of diameter on thrust: thrust increases with rotational speed and, for the same speed, thrust increases with diameter. The thrust of APC 8045 has no significant change when the rotational speed is less than 5,000 r/min, the thrust of APC 9045 and APC 1145 has no significant change when the rotational speed is less than 4,000 r/min, and the thrust of APC 1245 has no significant change when the rotational speed is less than 3,000 r/min. When the diameter of propeller varies from 8 inches (203.2 mm) to 9 inches (228.6 mm), the increase of thrust is significant, and the thrust reaches a maximum difference of 7 N at 11,000 r/min; when the diameter of propeller varies from 11 inches (279.4 mm) to 12 inches (304.8 mm), the increase of thrust is not significant, and the difference of thrust remains about 1 N when the rotational speed is more than 6,000 r/min. We can speculate according to the above analysis. For the same rotational speed, when the diameter of propeller increases to a certain extent, the impact of further increase on thrust force is not significant. If more thrust is needed, a more powerful motor will be necessary to produce a higher rotational speed. The thrust of APC 9045 sharply increases and changes irregularly when the rotational speed is ~7,000 r/min, due to a resonance between the propeller and experimental platform; the other three propellers have no obvious resonances.

Among the propellers to be tested, those with a diameter of 9.0 inches (228.6 mm), i.e., APC 9045, APC 9060, and APC 9075, are chosen to deduce the effect of pitch on thrust; their parameters are shown in Table 4.

Figure 12 shows the effect of pitch on thrust. The thrust increases with increasing rotational speed, and at the same speed, the thrust increases with increasing pitch. The thrust of APC 9045, APC 9060, and APC 9075 have no significant change when the rotational speed is less than 4,000 r/min; and the thrust of these three types of propellers are almost the same when the rotational speed is less than 5,000 r/min. The difference of thrust between APC 9045 and APC 9060 remains about 2 N when the rotational speed is more than 7,500 r/min; the difference of thrust between APC 9060 and APC 9075 remains about 1.5 N when the rotational speed is more than 6,500 r/min. The thrust of APC 9045 sharply increases and changes irregularly when the rotational speed is ~7,000 r/min, due to a resonance between the propeller and experimental platform; the other two propellers have no obvious resonances. In Figure 9, we can see that the only resonance occurs for APC 9045, when the rotational speed is ~7,000 r/min. Considering the information from Figures 9 and 10 together, we can thus conclude that the rotational speed at which resonance occurs relates to diameter and not pitch.

3.2.2. Effects of Propeller Speed, Diameter, and Pitch on Torque. The propellers with a pitch of 4.5 inch (APC 8045, APC 9045, APC 1145, and APC 1245) are used to deduce the effect of diameter on torque.

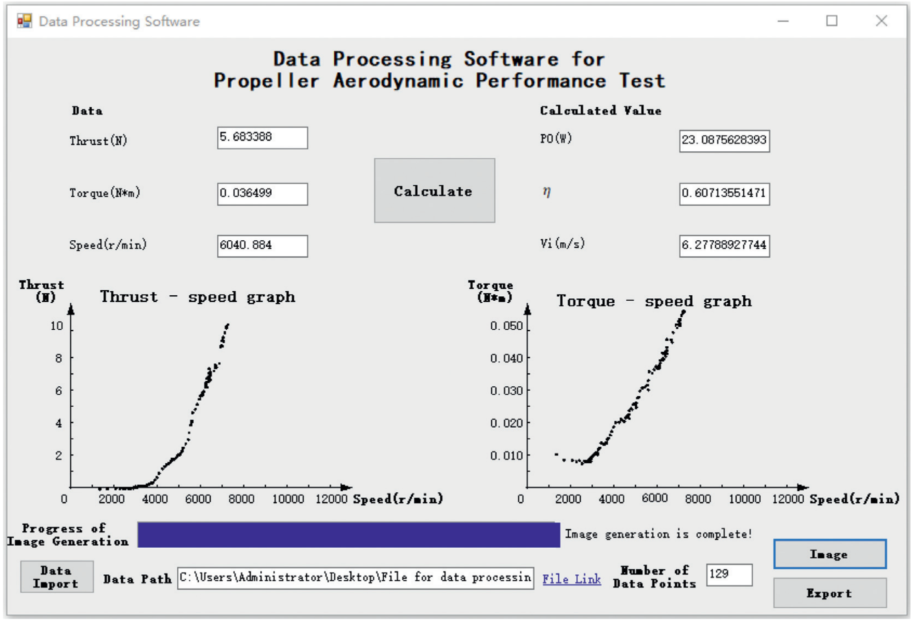

Figure 9: User interface of our data processing software.

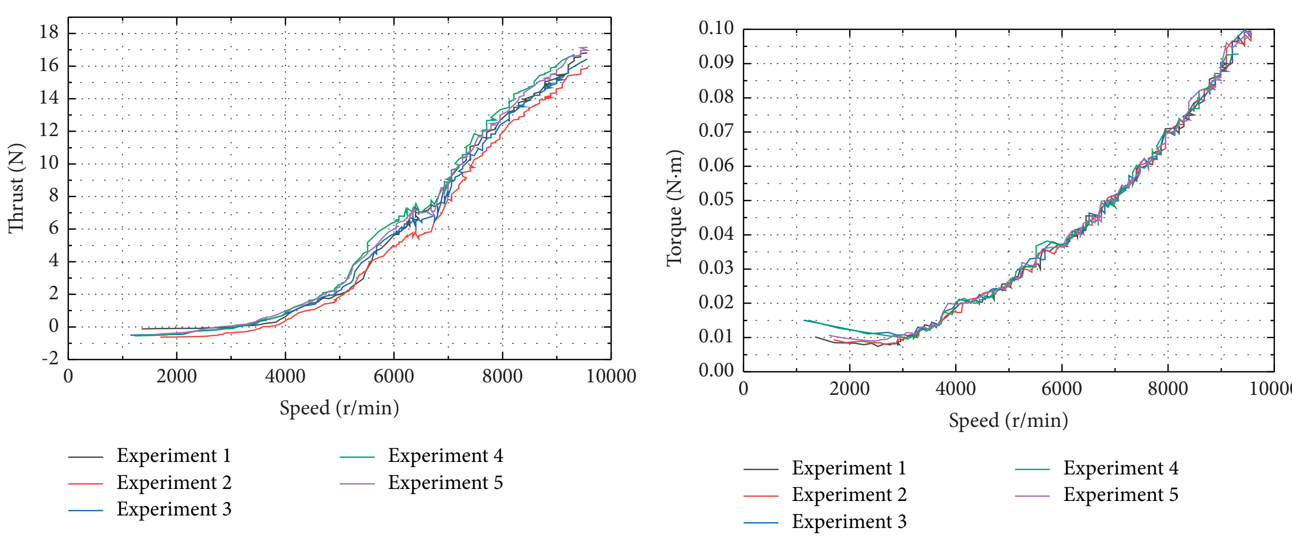

(a) (b)

Figure 10: Results of five repeated tests of the APC 1145 propeller: (a) thrust-speed graph and (b) torque-speed graph.

Table 3: Parameters for propellers with a pitch of 4.5 inches (114.3 mm).

Propeller	Diameter (mm)	Pitch (mm)
APC 8045	203.2	114.3
APC 9045	228.6	114.3
APC 1145	279.4	114.3
APC 1245	304.8	114.3

Figure 13 shows the effect of diameter on torque. The torque decreases at first then increases with rotational speed and, for the same speed, the torque increases with diameter. The torque of APC 8045 and APC 9045 decreases slowly with rotational speed when the rotational speed is less than 3,800 r/min and then increases rapidly when the rotational speed is more than 3,800 r/min; the torque of APC 1145 and APC 1245 decreases slowly with rotational speed when the rotational speed is less than 2,800 r/min and then increases rapidly when the rotational speed is more than 2,800 r/min. When the diameter of propeller varies from 8 inches (203.2 mm) to 9 inches (228.6 mm) or varies from 9 inches (228.6 mm) to 11 inches (279.4 mm), the increase of torque is significant; when the diameter of propeller varies from 11 inches (279.4 mm) to 12 inches (304.8 mm), the increase of torque is not significant. This variation of torque is similar to

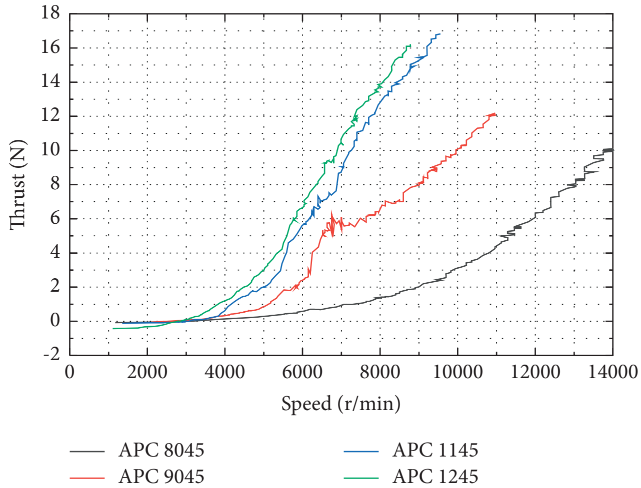

Figure 11: Effect of diameter on thrust.

Table 4: Parameters of propellers with a diameter of 9.0 inches (228.6 mm).

Propeller	Diameter (mm)	Pitch (mm)
APC 9045	228.6	114.3
APC 9060	228.6	152.4
APC 9075	228.6	190.5

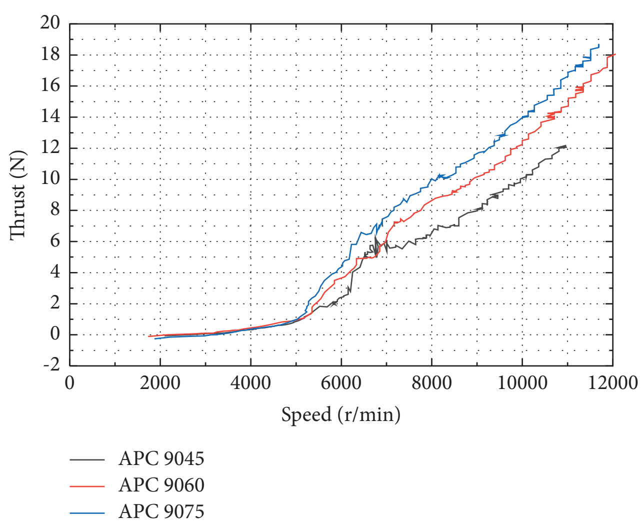

Figure 12: Effect of pitch on thrust.

that of thrust. The speed-torque curve is not smooth. The explanation for this phenomenon is that the torque produced by the propeller is small, so the vibration of the experimental platform has great influence on the torque measurement, which makes the continuity of the curve poor.

The propellers with a diameter of 9.0 inches (APC 9045, APC 9060, and APC 9075) are used to deduce the effect of pitch on torque.

Figure 14 shows the effect of pitch on torque. The torque decreases at first then increases with rotational speed and, for the same speed, the torque increases with pitch. The torque of APC 9045, APC 9060, and APC 9075 decreases slowly with rotational speed when the rotational speed is less than 3,800 r/min and then increases rapidly when the rotational speed is more than 3,800 r/min. The torque of APC 9060 and APC 9075 is practically the same when the rotational speed is less than 5,200 r/min. The torque difference of each propeller increases gradually, but the increase is not significant. As before, the continuity of the curves is poor. By comparing Figures 13 and 14, it is obvious that the diameter of the propeller has a greater influence on torque, while the pitch of the propeller has a smaller influence on torque.

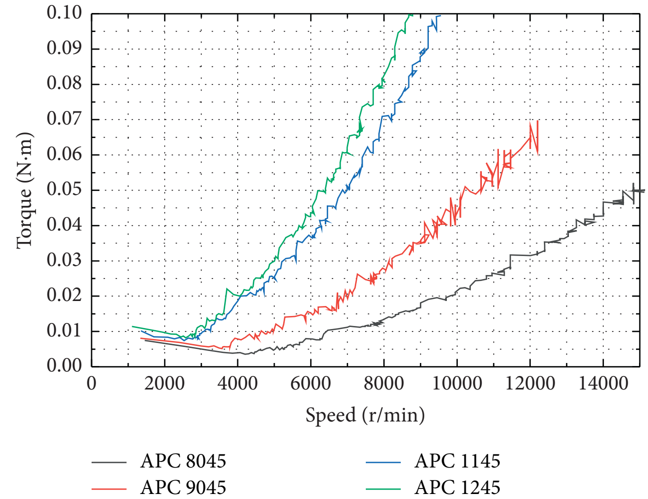

Figure 13: Effect of diameter on torque.

3.2.3. Effects of Propeller Speed, Diameter, and Pitch on C_{T0}. Static thrust coefficient C_{T0} is a parameter to evaluate the hover performance of propeller. C_{T0} can be calculated by equation (19), where D is the propeller diameter:

$$C_{T0} = \frac{T}{\rho \times n^2 \times D^4}. \tag{19}$$

The propellers with a pitch of 4.5 inch (APC 8045, APC 9045, APC 1145, and APC 1245) are used to deduce the effect of diameter on C_{T0}.

Figure 15 shows the effect of diameter on C_{T0}. C_{T0} of APC 8045 increases with rotational speed, while C_{T0} of APC 9045, APC 1145, and APC 1245 increases with rotational speed till the speed is ~6,500 r/min and then remains constant with a slight downward trend. This is because the range of speed is not wide enough to make C_{T0} of APC 8045 remain constant. C_{T0} of APC 8045 is the lowest in this group of experiment. When the rotational speed is less than 6,500 r/min, C_{T0} of APC 9045, APC 1145, and APC 1245 have no significant distinction; when the rotational speed is more than 6,500 r/min, C_{T0} of APC 9045, APC 1145, and APC 1245 decreases with diameter for the same speed. One possible reason for this phenomenon is that the motor does not provide enough torque to drive the propeller with large diameter. C_{T0} of APC 9045 sharply increases and changes irregularly when the rotational speed is ~6,500 r/min, due to

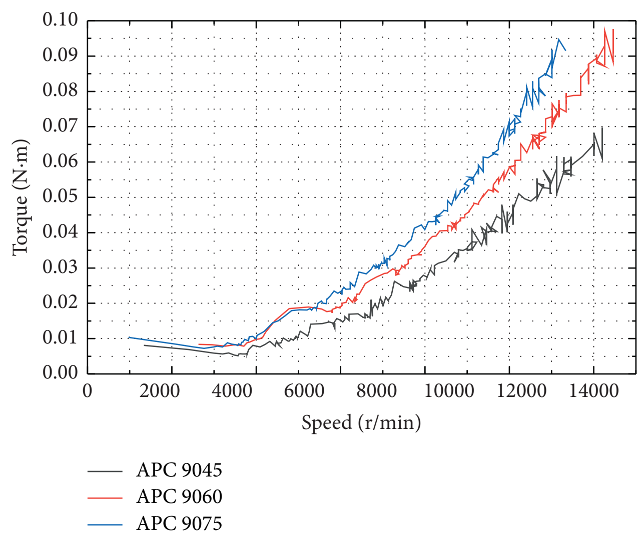

Figure 14: Effect of pitch on torque.

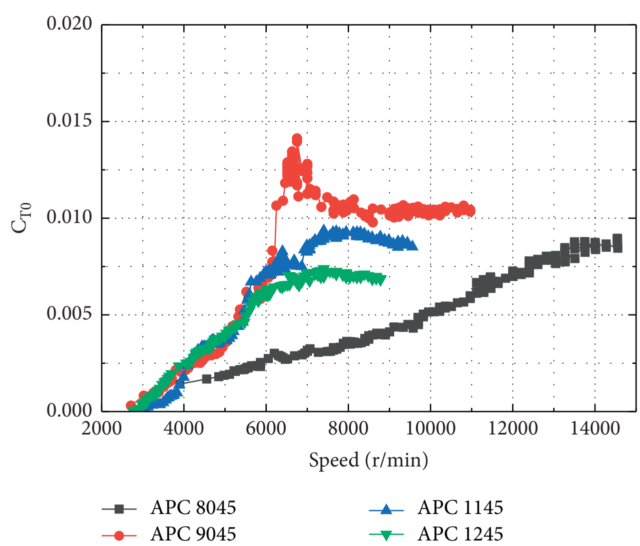

Figure 15: Effect of diameter on C_{T0}.

a resonance between the propeller and experimental platform; the other three propellers have no obvious resonances.

The propellers with a diameter of 9.0 inches (APC 9045, APC 9060, and APC 9075) are used to deduce the effect of pitch on C_{T0}.

Figure 16 shows the effect of pitch on C_{T0}. C_{T0} of APC 9045, APC 9060, and APC 9075 increases with rotational speed when the rotational speed is less than 6,500 r/min and then remains constant when the speed is more than 6,500 r/min. When the rotational speed is less than 6,500 r/min, C_{T0} of APC 9045, APC 9060, and APC 9075 has no significant distinction; when C_{T0} of APC 9045, APC 9060, and APC 9075 remains constant, it increases with pitch for the same speed. C_{T0} of APC 9045 sharply increases and changes irregularly when the rotational speed is ~6,500 r/min, due to a resonance between the propeller and experimental platform; the other two propellers have no obvious resonances.

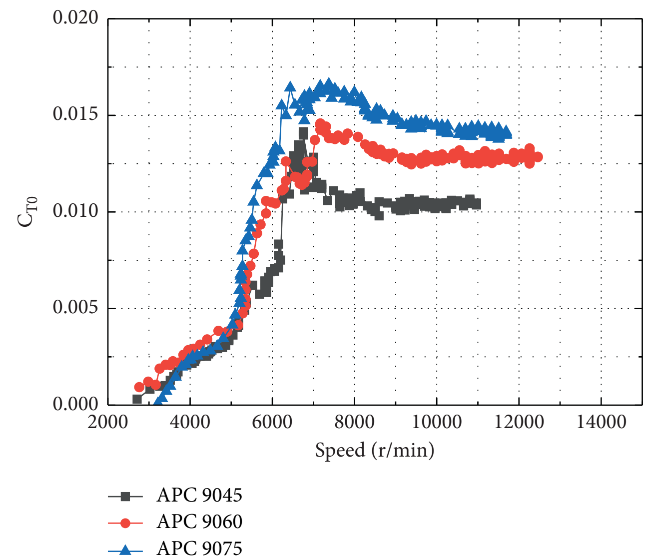

Figure 16: Effect of pitch on C_{T0}.

4. Conclusions

(1) We analyze the aerodynamic performance of propellers to calculate their thrust, drag, and power based on blade element momentum theory.

(2) A model of propeller aerodynamic performance is presented and verified by a calculated example. This model of propeller aerodynamic performance can determine feasible ranges of R and b on the basis of the airfoil and m.

(3) A design for a propeller aerodynamic performance experiment system is proposed, including its measurement and control system. We construct an experimental platform and test the aerodynamic performance of several propellers.

(4) Software is developed to process the data on propeller speed, thrust, and torque. The software can plot graphs of propeller thrust and torque against rotational speed and perform a single-step calculation of three parameters for a propeller: P_0, V_i, and η. We conclude that both thrust and torque increase with increasing speed, propeller diameter, and propeller pitch; C_{T0} increases with rotational speed and propeller pitch, but not with propeller diameter.

After referring to existing experimental platform, we design a new structure of sensor group including torque sensors, thrust sensors, and an infrared speed sensor. The new structure makes the propeller aerodynamic performance experiment system more accurate in torque measuring and more stable under the existing experimental conditions. The experimental data including propeller speed, thrust, and torque are used to analyze the aerodynamic performance of APC propellers. The propeller chosen for the experiment is the most commonly used type for UAVs, which makes the experimental data more convincing in assisting propeller selection for UAVs. And, we plan to test more types of propellers to build an aerodynamic performance database based on existing research, which will provide a higher reference value for propeller selection for UAVs.

By analyzing the experimental data, we find the experimental system has some deficiencies, including a certain extent effect from the load cell structure and the vibration of the experimental platform.

So, a few projects and recommendations for future work are listed below:

(1) Redesign the force measurement sensors to acquire a smaller structure, aiming at decreasing the blockage of the load cell structure behind the propeller

(2) Select sensors with higher accuracy to get more accurate experimental data

(3) Redesign the structure of the aluminum alloy frame to reduce the vibration and achieve the purpose of lightweight

(4) Design a variable-pitch propeller experimental platform based on this paper and study the effect of pitch on thrust, torque, and C_{T0} better

(5) In order not to be limited to the aerodynamic performance research of UAV in the hovering state, we will conduct further experiment under the condition of the wind tunnel to study the effect of speed, diameter, and pitch on thrust coefficient C_T and advance ratio J

Data Availability

The data used to support the findings of this study are included within the article.

Conflicts of Interest

The authors declare that there are no conflicts of interest regarding the publication of this paper.

Acknowledgments

This research was supported in part by Jilin Province Development and Reform Commission, under Grant 2020C018-2, and Jilin Province Key R&D Plan Project, under Grant 20200401113GX.

Supplementary Materials

Supplemental files include Data of Figures and File for data processing software (APC 1145). (*Supplementary Materials*)

References

[1] Q. Quan, *Introduction to Multicopter Design and Control*, Springer Singapore, Singapore, 2017.

[2] Y. Guo, J. Guo, C. Liu, H. Xiong, L. Chai, and D. He, “Precision landing test and simulation of the agricultural UAV on apron,” *Sensors*, vol. 20, no. 12, p. 3369, 2020.

[3] W. H. Maes and K. Steppe, “Perspectives for remote sensing with unmanned aerial vehicles in precision agriculture,” *Trends in Plant Science*, vol. 24, no. 2, pp. 152–164, 2019.

[4] G. Yang, J. Liu, C. Zhao et al., “Unmanned aerial vehicle remote sensing for field-based crop phenotyping: current status and perspectives,” *Frontiers of Plant Science*, vol. 8, p. 1111, 2017.

[5] J.-C. Trujillo, R. Munguia, S. Urzua, E. Guerra, and A. Grau, “Monocular visual SLAM based on a cooperative UAV-target system,” *Sensors*, vol. 20, no. 12, p. 3531, 2020.

[6] S. Siebert and J. Teizer, “Mobile 3D mapping for surveying earthwork projects using an Unmanned Aerial Vehicle (UAV) system,” *Automation in Construction*, vol. 41, pp. 1–14, 2014.

[7] H. Shakhatreh, A. H. Sawalmeh, A. Al-Fuqaha et al., “Unmanned aerial vehicles (UAVs): a survey on civil applications and key research challenges,” *IEEE Access*, vol. 7, pp. 48572–48634, 2019.

[8] M. Muehlebach and R. D’Andrea, “The Flying Platform - a testbed for ducted fan actuation and control design,” *Mechatronics*, vol. 42, pp. 52–68, 2017.

[9] T. Jin, C. Yan, C. Chen, Z. Yang, H. Tian, and J. Guo, “New domain adaptation method in shallow and deep layers of the CNN for bearing fault diagnosis under different working conditions,” *International Journal of Advanced Manufacturing Technology*, pp. 1–12, 2021.

[10] E. Fresk, *Modeling, Control and Experimentation of a Variable Pitch Quadrotor*, Ms. thesis, Luleå University of Technology, Luleå, Sweden, 2013.

[11] A. Pretorius and E. Boje, “Design and modelling of a quadrotor helicopter with variable pitch rotors for aggressive manoeuvres,” *IFAC Proceedings Volumes*, vol. 47, no. 3, pp. 12208–12213, 2014.

[12] X. Dai, Q. Quan, J. Ren, and K.-Y. Cai, “Efficiency optimization and component selection for propulsion systems of electric multicopters,” *IEEE Transactions on Industrial Electronics*, vol. 66, no. 10, pp. 7800–7809, 2018.

[13] D. Lawrence and K. Mohseni, “Efficiency analysis for long duration electric MAVs,” in *Proceedings of Infotech@ Aerospace*, p. 7090, Arlington, Virginia, September 2005.

[14] M. Achtelik, K. M. Doth, D. Gurdan, and J. Stumpf, “Design of a multi rotor MAV with regard to efficiency, dynamics and redundancy,” in *Proceedings of AIAA Guidance, Navigation, and Control Conference*, p. 4779, Minneapolis, Minnesota, August 2012.

[15] W. Zhang, M. W. Mueller, and R. D’Andrea, “Design, modeling and control of a flying vehicle with a single moving Part That can Be positioned anywhere in space,” *Mechatronics*, vol. 61, pp. 117–130, 2019.

[16] R. Macneill and D. Verstraete, “Blade element momentum theory extended to model low Reynolds number propeller performance,” *Aeronautical Journal*, vol. 121, no. 1240, pp. 835–857, 2017.

[17] M. Mccrink and J. W. Gregory, “Blade element momentum modeling of low-re small uas electric propulsion systems,” in *Proceedings of 33rd AIAA Applied Aerodynamics Conference*, p. 3296, Dallas, TX, June 2015.

[18] R. Gill and R. D’Andrea, “Propeller thrust and drag in forward flight,” in *Proceedings of IEEE Conference on Control Technology and Applications (CCTA)*, pp. 73–79, IEEE, Kohala Coast, Hawai’i, August 2017.

[19] C. W. Stahlhut, *Aerodynamic Design Optimization of Proprotors for Convertible-Rotor Concepts*, University of Maryland, College Park, 2012.

[20] L. Prandtl, *Applications of Modern Hydrodynamics to Aeronautics*, Springer, Dordrecht, Netherlands, 1921.

[21] S. Goldstein, “On the vortex theory of screw propellers,” *Proceedings of the Royal Society of London - Series A:*

Containing Papers of a Mathematical and Physical Character, vol. 123, no. 792, pp. 440–465, 1929.

[22] B. A. Moffitt, T. H. Bradley, D. E. Parekh, and D. N. Mavris, "Validation of vortex propeller theory for uav design with uncertainty analysis," in *Proceedings of 46th AIAA Aerospace Sciences Meeting and Exhibit*, p. 406, Reno, Nevada, January 2008.

[23] P. Doerffer and O. Szulc, "Numerical simulation of model helicopter rotor in hover," *TASK Quarterly*, vol. 12, no. 3, pp. 227–236, 2008.

[24] K. Siddhardha, "Autonomous reduced-gravity enabling quadrotor test-bed: design, modelling and flight test analysis," *Aerospace Science and Technology*, vol. 86, pp. 64–77, 2019.

[25] T. T. Mac, C. Copot, R. D. Keyser, and C. M. Ionescu, "The development of an autonomous navigation system with optimal control of an UAV in partly unknown indoor environment," *Mechatronics*, vol. 49, pp. 187–196, 2018.

[26] A. M. Harrington, *Optimal Propulsion System Design for a Micro Quad Rotor*, Ph.D. dissertation thesis, Department of Aerospace Engineering, University of Maryland, College Park, Maryland, 2011.

[27] V. S. Chipade, Abhishek, M. Kothari, and R. R. Chaudhari, "Systematic design methodology for development and flight testing of a variable pitch quadrotor biplane VTOL UAV for payload delivery," *Mechatronics*, vol. 55, pp. 94–114, 2018.

[28] Z. Czyż and M. Wendeker, "Measurements of aerodynamic interference of a hybrid aircraft with multirotor propulsion," *Sensors*, vol. 20, p. 3360, 2020.

[29] Y. Lei and M. Cheng, "Aerodynamic performance of hex-rotor UAV considering the horizontal airflow," *Applied Sciences*, vol. 9, no. 22, p. 4797, 2019.

[30] P. M. Park, O. S. Hwang, Y. M. Kim, C.-T. Kim, and K.-J. Kwon, "Wind tunnel test on propellers for middle size electric propulsion uav," in *Proceedings of the Korean Society of Propulsion Engineers Conference*, pp. 784–788, The Korean Society of Propulsion Engineers, Pusan, South Korea, 2011.

[31] J. Fleming, T. Jones, and W. Ng, "Improving control system effectiveness for ducted fan VTOL UAVs operating in crosswinds," in *Proceedings of 2nd AIAA" Unmanned Unlimited" Conf. And Workshop & Exhibit*, p. 6514, San Diego, California, September 2003.

[32] G. Andres, S. Juan, L. Omar, C. Laura Suárez, and A. E. Jaime, "Numerical and experimental estimation of the efficiency of a quadcopter rotor operating at hover," *Energies*, vol. 12, no. 2, p. 261, 2019.

[33] S. R. Kesler, *Propeller Thrust Analysis Using Prandtl's Lifting Line Theory: A Comparison between the Experimental Thrust and the Thrust Predicted by Prandtl's Lifting Line Theory*, Ph.D. Dissertation thesis, Department of Mechanical Engineering, University of Utah, Salt Lake City, Utah, 2014.

[34] "AirfoilTools.com," Accessed on: Jan. 17, 2020 [Online]. Available: 2020, http://airfoiltools.com/airfoil/details?airfoil=n0012-il.

[35] "APC Propellers.com," Accessed on: Jan. 25, 2020 [Online]. Available: 2020, http://apcprop.com/Articles.asp?ID=255.